

Comparing One- and Two-way Quantum Repeater Architectures

Prateek Mantri¹, Kenneth Goodenough², and Don Towsley³
{¹pmantri, ²kgoodenough, ³towsley}@cs.umass.edu

*Robert and Donna Manning College of Information and Computer Sciences,
University of Massachusetts, Amherst, MA, USA 01002*

Abstract

Quantum repeaters are an essential building block for realizing long-distance quantum communications. However, due to the fragile nature of quantum information, these repeaters suffer from loss and operational errors. Prior works have classified repeaters into three broad categories based on their use of probabilistic or near-deterministic methods to mitigate these errors. Besides differences in classical communication times, these approaches also vary in technological complexity, with near-deterministic methods requiring more advanced technology. Recent increases in the number of available memories, and introduction of entanglement generation through multiplexing motivate a re-comparison of one-way and two-way repeater architectures. In this work, we propose a novel protocol that optimizes multiplexed elementary link generation and distillation in memory-unconstrained ‘connection-oriented’ two-way repeaters to boost the entanglement generation rates. We introduce a recursive formulation to derive the probability distribution of the number of Bell pairs in multiplexed two-way repeater architectures, compatible with probabilistic n -to- k distillation protocols. We then compare the performance of this new protocol with one-way schemes in the parameter regime where one-way schemes have previously been shown to be advantageous, and find that the multiplexed two-way protocol provides better performance with lower resource and technology requirements.

1 Introduction

Quantum communications have applications in quantum sensing [1–4], distributed quantum computing [5, 6], secure communications [7, 8], and quantum secret sharing [9, 10] among others. Furthermore, with the rise of quantum computers, a need for a network connecting different parties or nodes capable of supporting quantum information transfer is becoming critical.

However, transmitting quantum information over long distances poses significant challenges, primarily due to losses that grow exponentially with distance in optical fibers. Unlike classical communication, quantum networks cannot employ ‘receive and re-transmit’ strategies because of the no-cloning theorem, which prohibits the duplication of unknown quantum states. Prior studies have established fundamental limits on direct quantum information transmission [11, 12], underscoring the need for innovative solutions such as quantum repeaters.

Quantum repeaters are specialized devices designed to extend the range of quantum communications by dividing long segments into shorter segments, thereby mitigating losses through specific quantum gate and measurement operations. These devices significantly enhance the viability of long-distance quantum communications by employing shorter, manageable links to create extended connections. However, the implementation of these operations is fraught with errors, which can restrict the effective distance for practical quantum communication. To address both loss and operational errors, researchers have proposed various probabilistic (heralded generation and distillation operations) and near-deterministic (quantum error correction) approaches. These strategies have led to the development of three generations of quantum repeaters, each with distinct characteristics and technological requirements [13, 14].

First generation architectures use probabilistic entanglement generation to mitigate loss errors, and heralded entanglement purification (often probabilistic) to mitigate operational errors. Similar to the first generation, second generation schemes also use probabilistic heralded entanglement generation. However, second generation

uses near-deterministic quantum error correction to correct operation errors instead of probabilistic heralded purification. Third generation solely relies on near-deterministic quantum error correction schemes to correct both operation and loss errors. The probabilistic solutions, while more feasible with current technology, necessitate heralding and consequently suffer from increased temporal costs associated with classical communication. In contrast, quantum error correction-based approaches typically employ one-way signaling and have the potential to achieve higher secret-key rates. In this manuscript, we focus on the first generation (referred to in this manuscript as the two-way schemes) and the third generation (referred to as the one-way schemes) quantum repeater architectures.¹

To be viable, one-way schemes typically require almost perfect operations, along with complex encoding and decoding circuitry with a large number of measurement and gate operations. Moreover, to be able to correct for fiber loss errors, one-way schemes also require repeaters to be more closely spaced compared to two-way schemes [15, 16]. This duality in approach necessitates a detailed evaluation to determine the optimal strategy for different parameter regimes. With comparatively higher technological and resource costs, it also becomes important to see if the purported gains associated with the complex technologies of the one-way scheme can be achieved using relatively simpler technologies of the two-way scheme.

This motivates a thorough comparison between different quantum repeater approaches. In their pivotal work, Muralidharan *et al.* [14] performed a comprehensive comparison of the three generations of quantum repeaters, highlighting coupling efficiency (η_c), gate errors (ϵ_G), and gate times (t_G) as critical parameters for evaluation. They identified the specific parameter regimes where each generation excels. However, as quantum technologies advance, revisiting these comparisons with updated models and technologies is essential to ensure accurate assessments and practical implementations.

One example of advances in quantum technology has been in the area of long-lived memories [17–19] - something critical for two-way schemes to be viable for longer distances. While some implementations of one-way repeater architectures might also require long-lived memories when having slow gates, two-way schemes necessarily require long-lived memories that can outlive the classical communication time for confirming successful operations. Most prior analyses of two-way repeater schemes have focused on scenarios where memory availability is highly constrained, making memories the most significant cost factor [14, 20]. This focus has shaped the strategy of using multiplexing to maximize the success probability of at least one successful link per segment² [14, 21–23]. However, some studies have explored multiplexing with multiple simultaneous successes (for each elementary segment in a single shot) in mind [20, 24–27]. However, most of these studies analyze throughput in the context of linear-chain quantum networks with probabilistic swapping realized through optical circuits, but without any distillation capabilities. In such networks, a nested swapping schedule has no added benefit. In the cases where nested distillation schemes have been considered in the context of multiple-success multiplexing, deterministic distillation protocols are often used to simplify calculations [20, 25]. Some protocols also employ blind operations³ when considering a nested swapping schedule, simplifying the computation of the number of Bell pairs delivered and the time required [20, 25]. However, to the best of our knowledge, a detailed comparison between one-way and multiplexed two-way protocols has not been conducted.

In this manuscript, we investigate the performance differences between multiplexed two-way (first generation) and one-way (third generation) repeater architectures in parameter regimes that one-way repeaters are stipulated to provide better performance. We propose a nested swapping protocol for the memory unconstrained regime with distillation scheduling that can be adapted for different service metrics like secret-key rate or fidelity thresholds. For this protocol, we analytically track the probability distribution of the number of available pairs at each step of the protocol. Using this, we compare different repeater architectures using several appropriate performance metrics.

This manuscript is organized as follows. In Section 2, we introduce the two repeater architectures, in Section 3, we introduce the evaluation design outlining the parameter space, followed by Sections 4, and 5 where we present our evaluation of these protocols, and conclusions respectively. This is followed by a discussion of our

¹As a special case, we also include a particular variant of the second generation networks that use multiplexing for maximizing single elementary link success but no error correction to protect against operation noise.

²This kind of scheme has also been referred to as the second generation without encoding or ‘2G-NC’ [14]

³In blind mode, the repeater does not wait for classical information to arrive to proceed further, typically achieved at the cost of exponentially decreasing success probability.

findings and an outlook on potential future work. In the Appendix, we include our process models (Appendix A), and present a recursive formulation (Appendix B) to keep track of the probability distribution of the number of Bell pairs for different steps of our protocol.

2 System Description

2.1 Two-way repeater architecture

In this manuscript, we consider a linear network with each repeater station being equipped with a large number of optically active memories or emitters. These memories emit photons, which are then sent to a station located at the midpoint of the link connecting the two repeater stations. At this midpoint station, photons from two different repeaters are entangled and measured together, effectively creating a Bell pair link shared between the repeaters (See Figure 1).

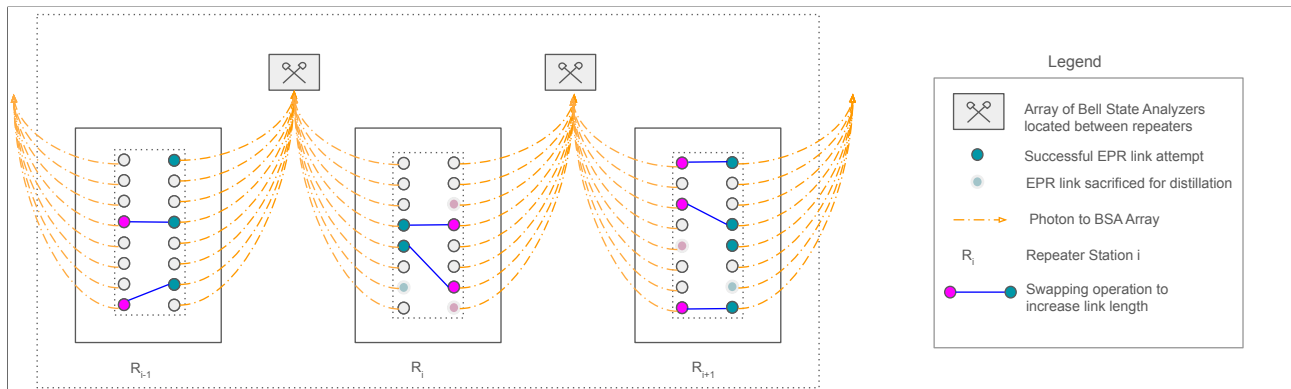


Figure 1: A schematic of the multiplexed two-way repeater scheme. Each repeater (denoted R_i etc.) has multiple emitter memories located on both sides. Each of these memories emit photons creating a spatially or spectrally multiplexed burst. At the mid-point between any two repeaters, an array of Bell state analyzers exist to entangle photons coming from both sides. Only a fraction of photons from either side survives the journey and reach the mid-point station.

2.1.1 Multiplexing for exactly one success across the network (2G-NC)

Multiplexing is a well known technique in telecommunications and computer networks, where multiple information channels are combined over a shared medium. Multiplexed quantum repeaters can be used to overcome the probabilistic loss errors associated with signal decay in optical fibers. This is achieved by attempting multiple Bell pair generation attempts in parallel through either spatial, time-bin, or frequency multiplexing. Due to poor rates associated with entanglement generation sources, various proposals have been made over time for the use of multiplexing to improve rates in quantum repeaters [28–30]. The most basic of these proposals involve parallelizing operations and sending multiple photons over an optical fiber (using time-division, spectral or spatial multiplexing), performing Bell State Measurements (BSMs), effectively creating entanglement between multiple matter qubits. To simplify analysis, these techniques often focus on using multiplexing to maximize the success of at least one Bell pair, with only one Bell pair kept between repeaters in the event of multiple successes. Moreover, this technique requires spatial or temporal multiplexing, which are often realized using lossy optical switches adding further loss [22]. However, a recent proposal by Chen *et al.* [30] uses spectral multiplexing and parallel entanglement creation to achieve high transmission rates without the added losses usually incurred from spatial or temporal multiplexing methods.

Another line of thought has explored multiplexing for quantum networks in multiple degrees of freedom (DOF) of a single photon [29, 31]. This scheme uses a single photonic pulse to entangle multiple pairs of

remote memories, minimizing the need for extensive spatial channels and precise temporal coordination. These proposals simplify the infrastructure needs while enhancing the rate at which entangled pairs can be generated in a quantum network. Furthermore, these techniques have also been extended to one-way schemes [32, 33].

Muralidharan *et al.* 2016 [14] categorizes the former approach of using multiplexing in two-way schemes to maximize the probability of success of at least one Bell pair in every segment as the ‘second generation without encoding’ (or 2G-NC). The focus of this technique is mostly to improve the success probability of creating exactly one Bell pair between neighboring repeater stations (see equation (B.15) in Appendix B.I). This approach has been shown successful in moderate to low gate errors when used in a low coupling regime. Note, as presented in [14], we do not extend the feature of distillation (see section 2.1.5) to the 2G-NC scheme.

2.1.2 Multiplexing for more than one success

In this manuscript, we primarily focus on multiplexing schemes that allows for creation of multiple Bell pairs across segments at the same time or with insignificant time delay⁴ achieved through spatial, spectral or time-division multiplexing. The primary emphasis, however, lies not in generating a single link per segment, but to use multiplexed channels to generate multiple elementary links – effectively reducing the inefficiencies associated with the basic multiplexing scheme. This enhancement allows us to balance the qubit resources required in one-way repeaters vis-à-vis two-way repeaters.

While multiplexing can enhance delivery rates, the number of end-to-end Bell pairs that can be delivered decreases as the number of segments increase in a linear relay network. Figure 2 shows the expected number of end-to-end Bell pairs that can be delivered in a single shot for a linear quantum relay network with deterministic swapping operations, for varying number of segments. The yellow dashed line denotes an approximate number of end-to-end Bell pairs by the quantity $M \cdot \pi_0$, where M is the multiplexed channels and π_0 is the elementary link success probability. This quantity has been used by some prior analysis [25] as an upper bound for the expected Bell pairs a quantum relay network can deliver. As evident from Figure 2, keeping track of the probability distribution allows us to provide a more precise expectation of output Bell pairs than the models considered in prior works.

Another important consideration is that end-to-end links created using a relay approach will potentially suffer a decay in fidelity owing to swapping operations - we address this in 2.1.4). To deliver as many high-fidelity end-to-end Bell pairs as possible, one may need to consider distillation operations (See Section 2.1.5). However, distillation schemes like DEJMPS are inherently probabilistic with success rates dependent upon the fidelity of the input Bell pairs. This makes an exact analysis difficult. To calculate and optimize repeater schemes, it is important to determine the probability distribution of the number of successfully distilled pairs at each step. We model the number of available Bell pairs as a random variable, with a distribution affected by non-deterministic operations (See equations (B.14) and (B.23) in Appendix B).

In Appendix B, we present a recursive formulation that builds upon the idea of tracking probability distributions and incorporates additional elements such as distillation (see section 2.1.5) and nested swapping (see section 2.1.4). This formulation provides a more comprehensive framework for modeling the dynamics of Bell pair generation, distillation, and swapping, allowing for a detailed analysis of the overall system performance. By integrating these elements, our recursive approach offers a significant improvement over previous models, enabling more accurate predictions and better optimization of quantum communication protocols.

2.1.3 Elementary link generation

In this setup, we use a meet-in-the-middle protocol with spatial (or spectral) multiplexing. Each repeater has an ensemble of emitters located on either side. This ensemble has a generation frequency ν , where it generates M photons entangled with M emitters in ν^{-1} time. This generation cycle of producing M multiplexed pairs in ν^{-1} time is referred to as a *burst*. One photon from each entangled photon pair thus generated is then sent to a Bell state analyzer located exactly midway between any two repeater stations hereinafter referred to as the midpoint analyzer. We further assume emissions are synchronized across the chain, and the photons arrive at the midpoint

⁴By insignificant time delay we mean time difference between entangled photons arrival at the midpoint station is significantly small compared to the elementary link propagation delay, and memory decoherence times.

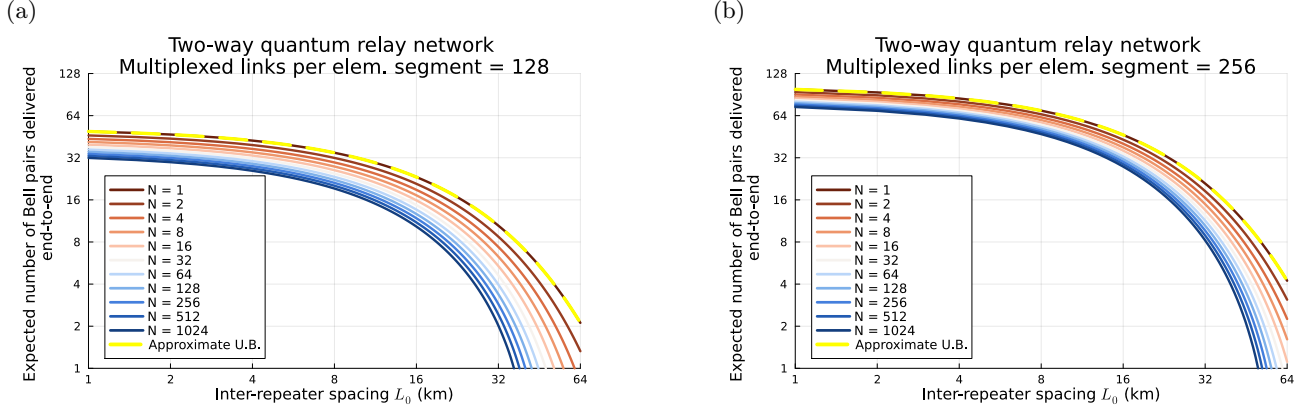


Figure 2: Expected number of surviving Bell pairs in a single shot versus inter-repeater distance for a quantum relay network with (a) 128 and (b) 256 multiplexed elementary links. The y-axis denotes the expectation of the minimum number of Bell pairs generated across all segments. With deterministic swapping operations, the minimum number of Bell pairs across segments also translates into the number of Bell pairs delivered end-to-end. The x-axis denotes the inter-repeater spacing, and N denotes the number of segments. The yellow dashed line shows an upper bound used by prior analyses to approximate the number of Bell pairs delivered.

station at the same time, and are able to effectively remove the ‘which-path-information’. The midpoint analyzer then performs parallel BSs on all M incoming photons from each side with a success probability of $1/2$, and communicates the result to both repeater stations. There is also a need for an optical switch to separate the various multiplexing modes to the respective detectors at the analyzers. This switching operation could be lossy depending on the multiplexing or the detectors used. Recent advances in detection technology [34] have shown promise for building large detector arrays with spatial resolution that can potentially allow us to forego the need for optical switches. While an explicit analysis has not been done, our proposed protocol is also compatible with a mid-point source (MPS) scheme like Zero-Added Loss Multiplexing (ZALM) [30], and will provide similar results. We also assume that time-bin dual-rail encoding is used for each multiplexed channel primarily since it allows for protection against depolarization of the photon in the channel. However, if a polarization-based encoding is used, the elementary link generation equations will have to be updated to accommodate relevant noise models.

2.1.4 Link Propagation

Two-way repeaters use a swap operation for link propagation. A swap operation involves performing a controlled NOT (CNOT) gate on the halves of two Bell pairs situated at a middle repeater, and measuring the involved qubits at the middle repeater to create a longer link. Depending upon the technology used, this swap operation may be probabilistic or deterministic, however, for simplicity we only consider deterministic swapping operations in our setup.

In our protocol we use a nested swap strategy based on the Innsbruck Protocol [35, 36]. The Innsbruck protocol involves a series of entanglement swaps where qubits initially entangled with nearby nodes are used to establish entanglement with more distant nodes through intermediary swaps. This yields a nested structure where the network is divided into $N = 2^n$ segments (see Figure 3). This nested swap procedure allows for the establishment of long-range entanglement connections between nodes that are not directly adjacent. By recursively applying entanglement swap operations, the protocol facilitates the generation of entangled links across the entire network. Prior works have studied swapping schedules other than nested swapping like Swap ASAP [37, 38], sequential generation and swapping [38, 39], hybrid strategies [40] among others. However, nested schemes perform better than several other swapping schemes especially in settings where the swapping operations are probabilistic, and repeaters are equipped with distillation, by providing an entanglement distribution rate

that decays polynomially rather than exponentially in distance [41]. Moreover, a nested swapping schedule allows for node synchronization for generation, swapping, and distillation operations. It is because of these reasons, coupled with an ease of analysis, that we have chosen a nested swapping schedule for our protocol.

Our protocol diverges from the standard Innsbruck protocol in two ways – (1) distillation may or may not be performed at each level depending on the expected quality of the Bell states (See Appendix B) (2) all links are created in parallel with multiple links shared between two stations, in a single burst with no interaction between bursts. In our protocol, we consider swaps as deterministic operations which allows us to save on the associated classical communication time costs. However, it is important to note that unless one has perfect elementary links, swaps even in the case of perfect gate and measurement operations, cause an exponential decay in the fidelity with each swap [42]. In the absence of a means to improve fidelity, this exponential decay makes quantum networks based solely on swaps impractical for long range communications. Appendices A.III, and A.IV explains the models used for gate and measurement operations, and equation (A.9) in Appendix A.VII has been used for modeling the swapping operations.

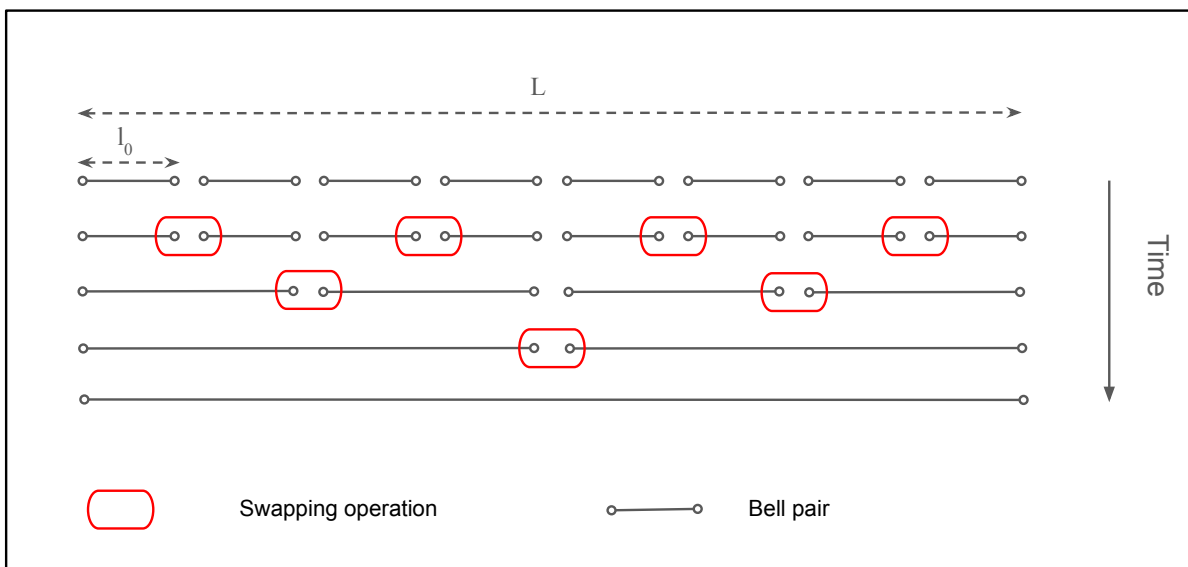


Figure 3: Schematic of a nested swapping protocol. We start with N elementary segments each of length l_0 . The red boxes represent a swapping operation. Based on the decision variable \mathcal{D}_i , distillation may be performed before a swapping operation. Each swapping operation doubles the length of the link. This process is repeated until an end-to-end link is established.

2.1.5 Distillation

The degradation in entanglement fidelity due to imperfect operations (like swaps) or imperfect memories used for storing the entangled qubits can be mitigated by using distillation or purification. In a distillation operation a larger number (n) of Bell pairs are sacrificed to achieve a smaller number (k) of higher fidelity Bell pairs. While significant improvements have been made in the field of distillation [43–46], in this paper, for ease of analysis, we use one of the basic schemes called the DEJMPS protocol ($n = 2, k = 1$) [47] (See equation (A.7) in Appendix A.VI). The DEJMPS protocol typically is employed in an iterative fashion until a threshold fidelity is achieved or a threshold number of Bell pairs have been exhausted to create a higher fidelity pair. However, since most of our evaluation focuses on high input fidelity Bell pairs, we have considered only a maximum of a single round of distillation before swapping. Our protocol is easily modified to account for multiple rounds of distillation i.e. performing as many distillation rounds until the fidelity of all available Bell pairs reach above

the threshold fidelity, or we run out of multiplexed Bell pairs available.

A critical consideration is the temporal overhead introduced by executing DEJMPS. In deterministic distillation protocols, classical communication is needed to relay Pauli correction information between parties. However, this exchange does not introduce latency, allowing operations to proceed without delay. In contrast, probabilistic distillation protocols impose stricter timing requirements, as the success or failure of the distillation must be communicated to determine subsequent actions. This requirement can create a significant bottleneck in two-way architectures. To address these temporal costs, one approach is to operate in a “blind” mode [36]. However, in our protocol, the distillation operations are conducted with “informed” decisions [20, 25].

Deterministic distillation protocols might offer better performance than the probabilistic protocols like DEJMPS on metrics such as secret-key rates and memory usage over time. However, deterministic distillation protocols typically require a large number of input entangled states for creating a higher fidelity state. Another possibility is to utilize a combination of deterministic distillation schemes with probabilistic but high fidelity yielding DEJMPS like protocols at higher nesting levels.

Another important consideration in two-way repeaters is the decision whether to distill or not before performing a swap. Given a higher initial fidelity, it is possible to perform multiple swaps, and increase the length of the link before the fidelity drops to a level where distillation might be required. At each level a decision must be made whether to perform distillation or not prior to performing a swap.

As discussed in Section 2.1.2, and further explained in Appendix B, it is possible to keep track of the probability distribution of the number of Bell pairs. This probability distribution can be further optimized over the decision to distill based on a key service metric like the secret-key rate per shot or fidelity threshold. In the proposed protocol, this decision parameter is pre-determined for all nested levels, and is taken to be a static network-wide agreement. This decision can be made using any rule that might be suitable to the application, and the metric to be optimized. As examples, we have included two case scenarios in our analysis for deciding when to perform distillation – (1) comparing expected secret-key rates with and without distillation for a chain with 2^{n-i} segments, where i is the nesting level, and $n = \log_2 N$ for an N elementary segment linear network (See equation (B.25) in Appendix B). This is primarily driven by the fact that secret-key rate combines both throughput and fidelity into a single metric making it a useful metric to optimize. This rule has been referred to in this manuscript as the SKR rule. (2) comparing the fidelity of links to a pre-determined fidelity threshold, where the decision to distill is contingent upon the link quality being less than the threshold (referred to in this manuscript as the F_{th} rule). This approach could potentially be useful in a scenario where the quality of links above a certain threshold is desired as a service metric [37]. Both of these policies can be further optimized with an objective to maximize the end-to-end secret-key rate or number of Bell pairs while considering various possible distillation schedules and protocols. Furthermore, since we consider distillation, we need to keep track of the Bell pairs sacrificed when a round of distillation is performed. For a general n' -to- k' distillation scheme, each successive distillation round reduces the number of available Bell pairs by a factor of $1/\lceil n'/k' \rceil$ - see equations (B.27) and (B.28) in Appendix B for details.

2.1.6 Quality of Memory

The temporal costs associated with classical communication with distillation requires Bell states to be held in long-lived memories that do not undergo significant decoherence. Degradation in memory quality is usually characterized by T_1 and T_2 times. The T_1 time denotes the thermal relaxation time - the time it takes for the excited state $|1\rangle$ to relax back to the ground state $|0\rangle$. The T_2 time is the dephasing time that captures the loss of coherence due to dephasing in a quantum memory. In this manuscript, we only consider dephasing noise (See Appendix A.V).

2.1.7 Termination

The protocol concludes once one or more Bell pairs are successfully established between the end stations. However, there may be cases where repeater stations lack enough Bell pairs to perform distillation. We explore various termination strategies for such scenarios when the number of Bell pairs in a segment drops below a certain threshold (R_i) for any nesting level i . If the static distillation schedule—predetermined based on a

distillation rule such as a fidelity threshold F_{th} or the *SKR* rule outlined in this manuscript—requires at least one round of distillation at the current or higher nesting levels, the protocol must adapt accordingly. Using this framework, we propose three potential termination strategies:

- **Strategy 1:** Repeater stations in the affected segment send classical messages instructing Alice, Bob, and all intermediate repeaters to halt all operations related to the burst. As these messages propagate, the repeater stations release the memory resources associated with the burst.
- **Strategy 2:** A variation of the first strategy involves the repeaters performing entanglement swaps and notifying their counterpart stations⁵ to perform additional swaps without distillation. This approach allows repeaters holding k links to proceed similarly, ultimately establishing k end-to-end links. However, because this strategy bypasses the static distillation schedule, the established links will likely be of lower quality.
- **Strategy 3:** Another option is to allow unaffected segments to proceed without interruption. Specifically, repeater stations can continue performing distillation and swapping operations in segments where the number of Bell pairs $k \geq R_i$. Repeater stations learn about the failure on a segment as and when they do, minimizing classical communication time compared to Strategy 1. Also, this strategy requires fewer resources than Strategy 2, reducing the need for gates and other operations, while freeing up memory for future bursts.

The threshold R_i can be set based on the minimum number of Bell pairs required for the chosen n' -to- k' distillation scheme (such that $R_i \geq n'$). Alternatively, this threshold may be optimized using the static distillation decision schedule, ensuring that termination does not occur at any nesting level. We have selected **Strategy 3** because it minimizes classical communication time, potentially avoids unnecessary gate and measurement operations, and frees up memory resources for future bursts. However, this strategy sets a lower bound on performance. While computationally challenging, a more efficient termination strategy that optimizes resource usage could be developed in future work.

2.2 One-way repeater architecture

First proposed by Munro *et al.* 2013 [48] and 2015 [13], the one-way repeater architectures uses near-deterministic methods to handle loss and operational errors.

One fundamental difference between this scheme and a two-way scheme is its requirement for only forward or one-way classical communication. This need for one-way classical communication can further be eliminated if recovery operations on the errors accumulated in the preceding segment are performed at each repeater, resulting in only forward flow of quantum information. To tackle errors, in a one-way scheme, the quantum state to be transmitted is encoded in a logical qubit (qudit) using several physical qubits (qudits). For our analysis, we only consider a Bell pair of which one qubit is encoded and transmitted, while the other stays with the initiating party. Depending upon the nature of errors, there are various quantum error correction codes that can be used to encode the Bell pair and protect against these specific anticipated errors. For our comparison, we focus on Quantum Parity Codes (QPCs) [15, 48]. QPCs are generalized Shor Codes, and are capable of supporting Teleportation Based Error Correction [49]. A general form of an (n, m) QPC encodes the logical qubits as $|0\rangle_L = (|+\rangle_L + |-\rangle_L)/\sqrt{2}$ and $|1\rangle_L = (|+\rangle_L - |-\rangle_L)/\sqrt{2}$, with

$$|+\rangle_L = \frac{1}{2^{n/2}}(|0\rangle^{\otimes m} + |1\rangle^{\otimes m})^{\otimes n}; |-\rangle_L = \frac{1}{2^{n/2}}(|0\rangle^{\otimes m} - |1\rangle^{\otimes m})^{\otimes n}.$$

QPCs can be used to recover any encoded state under erasure noise as long as the following two conditions are met - (1) at least one qubit must arrive for each sub-block; (2) at least one sub-block must arrive with no loss. QPCs are loss tolerant [50] which is particularly useful to counter erasure losses in the optical fiber. They can also be prepared fault tolerantly [15]. For a detailed explanation on syndromes in QPCs see Namiki *et al.* [51]. In our analysis, we assume the codes are prepared fault-tolerantly, and require the same setup as outlined in

⁵Counterparties refer to repeaters that share a Bell pair with the initiating repeater.

Muralidharan *et al.* 2014 [15] and Namiki *et al.* [51]. For simplicity, similar to the two-way protocol outlined earlier, we assume spatial multiplexing such that all incoming photons from a block arrive at the repeater at the same time or without any significant time delay. The scheme is compatible with spectral and time bin multiplexing, however with such model designs, associated switching losses might need to be considered. Furthermore, similar to the strategy outlined in [15], we use codes that deliver the highest key rate using the least number of qubits for our comparison.

3 Evaluation design

3.1 Parameter Regime

We develop a model of our protocol in Appendix B and use it to compare its performance with that of the one-way scheme. As mentioned in Section 2.1.5 and Appendix B, in our analysis we optimize the decision to perform distillation using a service metric (e.g. secret-key rate or fidelity threshold). Although the model yields entanglement delivery rate and average fidelity, we will use secret-key rate as our metric throughout this section. Our choice of secret-key rate as the primary performance metric is guided by the necessity of establishing a network capable of consistently delivering high-quality Bell pairs at a rapid pace. Secret-key rate combines fidelity (link quality) and entanglement delivery rate (quantity) into a single metric, making it a straightforward choice for measuring performance. See Appendix A.VIII for details.

In Figure 4, we show the secret-key rate of the multiplexed two-way protocol across different ranges of coupling coefficients, gate and measurement noise, for distances up to 10^4 km. We note that the coupling efficiency and gate errors affect secret-key rate in qualitatively different ways. Secret-key rate decreases as coupling efficiency decreases in a uniform manner over all segment lengths whereas increasing gate errors asymmetrically affects more segmented networks.

In this section we outline the parameter regime, and the model assumptions for the results presented in Section 4, where we compare the performance of multiplexed two-way protocol (MTP) with one-way schemes. For our comparison, we have selected different Quantum Parity Codes optimized for specific distances for different parameter settings of coupling efficiency, and gate and measurement noise. Furthermore, in our analysis we mainly focus on the parameter regime, demonstrated in prior works to be advantageous for one-way repeater schemes⁶.

For this comparison, keeping in line with the analysis in [14] we assume high initial fidelity (computed as $F = 1 - 1.125\epsilon_G$), gate error $\epsilon_G \in \{10^{-4}, 10^{-3}\}$, measurement error $\xi = 0.25\epsilon_G$, coupling coefficient $\eta_c \in \{1, 0.9\}$. Moreover, in this analysis we have chosen a realizable decoherence time with $T_2 = 1$ seconds. This parameter choice has been experimentally demonstrated in hardware platforms like trapped ions [53] and Rydberg atoms [54]. In our analysis we consider optimal architectures for both one- and two-way schemes. For the one-way scheme, for each distance, an optimal (n, m) QPC is chosen that minimizes the total number of qubits required to deliver unit secret-key, with the search parameters constrained to $n \leq 70, m \leq 20$ and the inter-repeater spacing constrained between 1 and 4 km. For the multiplexed two-way scheme (MTP), a maximum of 1024 segments, and 1024 multiplexed channels have been considered, primarily to limit computational costs. For 2G-NC, we use a numerical search for selecting the optimal number of multiplexed channels (ranging between 1 and 1024) that minimized the total number of qubits required over the linear network to deliver unit secret-key. Furthermore, to make this comparison, for both QPC and MTP, only the envelopes of the best performing configuration (in terms of inter-repeater spacing, and additionally for QPC the specific (n, m) code)⁷ have been considered.

3.2 Summary of assumptions

- Our protocol assumes unconstrained availability of quantum emitters/memories at all repeaters.

⁶As per Muralidharan *et al.* [14], the parameter regime where one-way should perform better than two-way is given by $\eta_c \geq 0.9, \epsilon_G \leq 10^{-3}, t_G \leq 10^{-9}$ s.

⁷Performance compared on the metric of Secret-key rate (SKR) per channel use per burst.

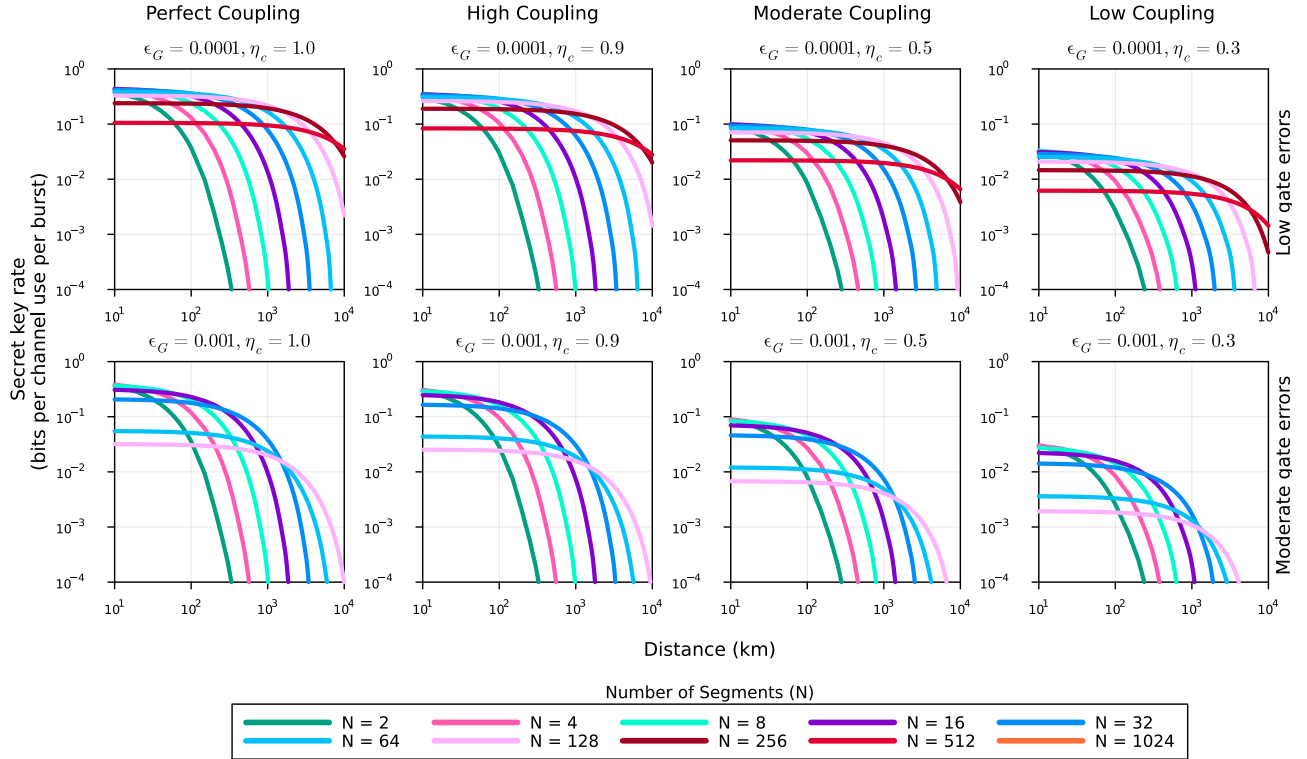


Figure 4: Performance of multiplexed two-way protocol (MTP) with distance using secret-key rate as the metric. The number of segments is shown in different colors and denoted by N . The plots in the top row consider a low gate error scenario with a gate error rate (ϵ_G) of 10^{-4} or 0.01%, and the bottom row plots show the performance with moderate gate errors ($\epsilon_G = 10^{-3}$ or 0.1%). The different columns show the performance in different coupling regimes, starting with a perfect coupling ($\eta_c = 1$), with the coupling coefficient reducing when moving from left to right ($\eta_c \in \{1, 0.9, 0.5, 0.3\}$). In this setup, we used the protocol based on one-way BB84 [52] Secret-key rate to inform the distillation decision making process, allowing a maximum of one round of distillation at any level of nesting. Also, in this setup, no distillation is performed at the end level of nesting.

- We assume high cooperativity for the cavity-enhanced memories. Cavities have shown promise in realizations of quantum networks [55, 56], enabling implementations of efficient multi-qubit gates [57–59], fast storage and readouts [60].
- We assume switching to be perfect, for both inter-memory connectivity at the repeater, and in case of spectral or temporal multiplexing, the switching required to connect incoming photons to the appropriate memory. Furthermore, we do not account for delays associated with performing CNOT gate operations between any two qubits. These delays costs can be non-trivial with current hardware technology especially if the relative distance between the selected qubits on the register is large. The primary reason for not accounting for these delays is that we assume fast gate operations for both one-way and two-way schemes. Both one-way and two-way schemes will be proportionally hit by temporal costs associated with these two-qubit gate operations.
- We assume detectors are perfect, and that the probability of success of a BSA is exactly 1/2 at the midpoint stations.
- We assume that detectors and quantum memories can be reset in a time smaller than the inverse of the source frequency ν . We further assume that qubit readout times are sufficiently fast such that they are

negligible with respect to the inverse of the source frequency ν . This allows for pipe-lined operations where the only bottleneck is the source’s ability to generate bursts.

- We assume that the optical losses in the fiber in transit to be the same for all frequencies in case spectral multiplexing is used. We further assume that the optical fiber does not contribute to any other form of noise except erasure. We assume the speed of light in fiber to be 200,000 km/s.
- We assume deterministic swap gates. Several proposals that use high cooperativity cavities have shown potential for achieving such gates [57, 61].
- Memory decoherence time T_2 is assumed to be 1s [17–19].
- We assume fast gate and measurement operations (gate and measurement time $t_G \ll 10^{-9}s$).
- Measurement errors ξ are assumed to be a quarter of gate errors ϵ_G i.e., $\xi = 0.25\epsilon_G$ [14].
- Elementary link fidelity is estimated to be $1 - 1.25\epsilon_G$ [14] using depolarized states for elementary link Bell pairs.
- Fiber attenuation length has been taken as 20 km.

3.3 Costs

Prior works have mostly focused on memory constrained regimes, and have considered memories as the most significant cost factor [14, 20, 25]. However, promising developments in multiple hardware platforms since [17, 18] have weakened these assumptions. It is critical that better cost metrics be considered to evaluate the performance of different repeater architectures. While a detailed cost analysis⁸ might be the most appropriate course of action, we believe the following can still be a guiding post for comparing any quantum network deployment -

- a) Cost of repeater installations including acquisition of land and physical infrastructure, maintenance, temperature requirements among others. This is captured in our metric of the number of repeaters required for delivery.
- b) Memory costs including initialization costs, and residence times⁹. Since both one-way and two-way repeater architectures require vastly different kinds of memories in the parameter regime of fast gate operations and readout, we capture these costs with the metric of number of qubits required for delivering one Bell pair.
- c) Number of 2-qubit gates, and circuit size and usage. In our analysis we have only considered 2-qubit gates as the appropriate measure, since both QPC and two-way nested schemes will require 2-qubit gate operations.
- d) Number of measurement operations. In [62], the authors identify the number of measurement operations as a potential candidate for evaluating link costs in the context of routing in quantum networks. The authors use simulations to establish the relationship between measurement count and overall network performance, highlighting this metric’s potential for assessing resource consumption when determining the optimal path for data transmission.
- e) Cost of operating a repeater including energy and maintenance costs. While we have not considered these in the current analysis, from a practical viewpoint these costs will be an important metric to consider. We leave this analysis for future work.

⁸A detailed evaluation would take into account noises from the environment - thermal and magnetic fluctuations etc.; hardware costs including refrigeration, fiber, etc; labor costs, physical infrastructure costs including land acquisition, building development and maintenance; software building and maintenance costs among other costs determining feasibility.

⁹Residence time is referred to as the amount of time a memory is engaged.

4 Results

4.1 Performance evaluation using secret-key rates

For comparing the performance using secret-key rate as the metric, we use two different flavors of the multiplexed two-way protocol (MTP) based on two different distillation decision rules - (1) rule based on secret-key rate (2) a rule based on fidelity threshold (Appendix B.II.1 and equation (B.25) for details). For the fidelity threshold, we have used the threshold of 0.95, based on a visual search on a small set of threshold values (See Supplementary Materials for performance plots using fidelity thresholds other than 0.95). As shown in Figure 5, the MTP repeater schemes outperform the protocol based on the optimal Quantum Parity Codes for all considered parameter regimes. These differences in performance range between one to two orders of magnitude depending upon the choice of gate errors and coupling efficiencies considered. In the case of moderate gate errors and long distances, understanding this gain in the context of associated costs, as analyzed in Section 4.2, is important. We also find that the MTP outperforms the multiplexing protocol aimed at single elementary link generation (referred to as 2G-NC in [14]) across the entire parameter regime considered in the manuscript. To note, both the SKR, and the $F_{th} = 0.95$ rule are probably non-optimal and an optimal distillation schedule can be achieved using a numerical search. Furthermore, since we have limited the number of distillation rounds to a maximum of one per nesting level, potential improvements in the performance could be made if this constraint is relaxed.

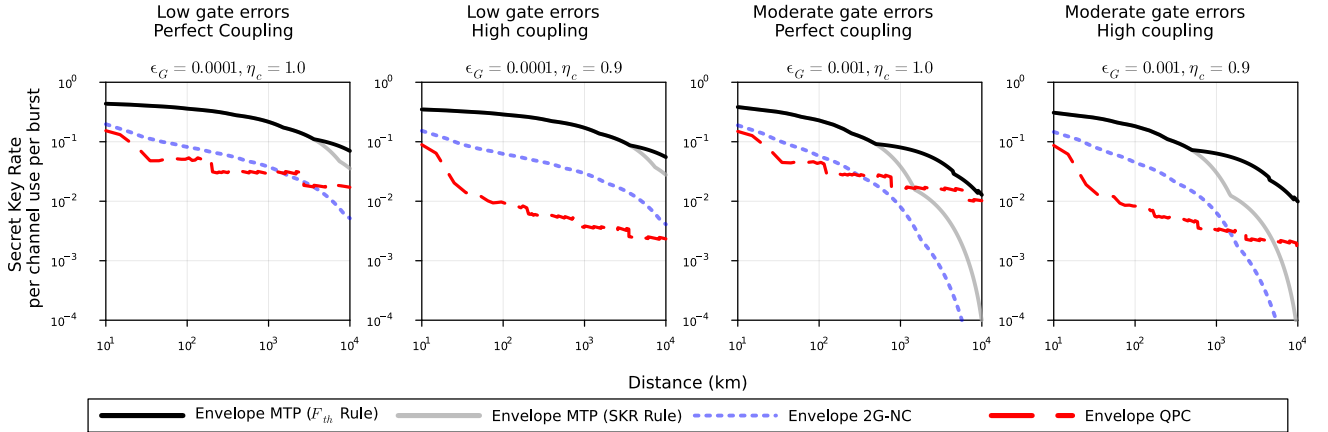


Figure 5: Performance comparison between one-way and two-way schemes using the secret-key rate as the metric. The red dashed line shows the performance by the optimal Quantum Parity Codes (QPC), the blue dotted line represents the optimal performance for the non-encoded second generation scheme ‘2G-NC’, the solid lines are the envelope for the secret-key rates for multiplexed two-way scheme (MTP) with two different distillation rules with black solid line representing the fidelity threshold rule, and the gray solid line representing the SKR rule. To note, for the fidelity threshold rule, we use $F_{th} = 0.95$. For both MTP schemes and the 2G-NC the envelope has been taken over with different number of elementary segments elementary varying between 2 and 1024 . For each distance, a specific (n, m) QPC is chosen optimizing for total number of qubits required with the search parameters constrained to $n \leq 70, m \leq 20$. For the MTP schemes and the 2G-NC, a maximum of 1024 multiplexed channels have been considered. Compared to the QPC and the 2G-NC, the MTP schemes deliver better secret-key rates per channel use per burst in all parameter regimes.

4.2 Comparison of resource costs

In this subsection, we compare different costs, i.e. the number of repeaters, number of 2-qubit gates, and number of measurement operations, associated with the one- and two-way repeater architectures. Figures 6, and 7 demonstrate that the resources required for the one-way schemes are significantly higher than the equivalently

multiplexed two-way schemes. Figure 6(a) compares the number of repeaters required for the optimal secret-key rates shown in Figure 5. As shown in the plots, the QPC based system requires a significantly larger number of repeaters compared to the multiplexed two-way (MTP) system. This difference in the required number of repeaters becomes more pronounced as imperfections in coupling and gate efficiency increase in the system. Note that 2G-NC requires slightly less or equal number of repeaters compared to the MTP schemes in most parameter regimes. In Figure 6(b), we compare the qubit resources required to deliver a unit secret-key for different gate and coupling efficiencies. In this analysis, we consider a lower bound on the number of qubit resources required for QPC, since we do not consider the ancilla qubits required for state preparation and teleportation-based error-correction. We observe from the graphs, that the QPC based system requires more qubit resources for all parameter regimes considered. However, if ancilla qubits are included, it is likely that the two-way scheme will perform even better. It should also be noted that the number of qubits required per unit secret-key delivered has been used as the metric of comparison in Muralidharan *et al.* 2016 [14]. Using the number of qubits required as the sole cost metric, it might be straightforward to see the attractiveness of the multiplexed two-way protocol compared to the QPC and the 2G-NC protocol. Figures 7(a) and (b) present the estimated number of measurement and 2-qubit gate operations per unit secret-key delivered required to maximize secret-key rate as a function of distance. As with the number of repeaters and qubits, we find that the QPC based one-way scheme requires significantly more gate and measurement operations across most parameter regimes considered with possible exception of low gate errors for distances $\lesssim 50$ km. For all other considered parameter regimes, these differences in gates and measurement costs range between one and two orders of magnitudes with the MTP posing lower resource requirements compared to both QPC and the 2G-NC.

5 Conclusion

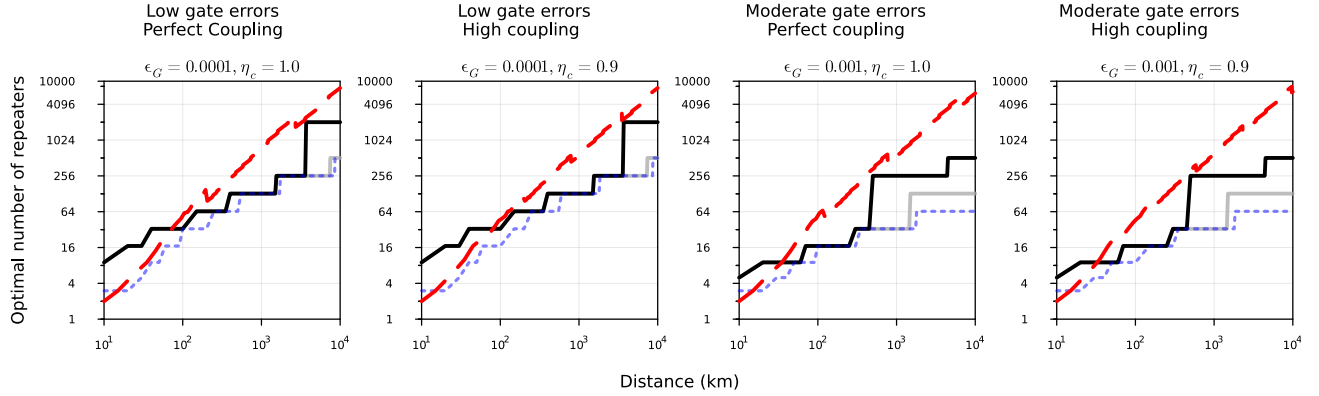
The rapid development of quantum technologies has spurred efforts to establish robust quantum networks. The choice of repeater architecture significantly impacts the scalability and reliability of these networks. A comprehensive comparison between different repeater architectures is essential to understand their strengths and weaknesses under different conditions, including error rates, resource availability, and communication latency. Such an analysis can guide the design of practical quantum networks by highlighting where specific architectures excel or falter, and providing insights into the trade-offs between performance and technological complexity.

Pioneering work by Muralidharan *et al.* [14] compared one-way and two-way schemes, identifying parameter regimes where each scheme could be advantageous. However, Muralidharan’s setup assumes a memory-constrained regime and does not utilize the full power of multiplexing. Studies considering multiplexing have focused on maximizing the success probability of a single elementary link or have not incorporated nested purification [14, 21–23]. Where such considerations have been made, distillation operations have often been assumed deterministic [20, 25]. This study aims to clarify the performance expectations of multiplexed two-way and one-way repeater architectures, providing a framework to make informed decisions when selecting the optimal architecture based on application requirements.

In this manuscript, we propose a two-way protocol that leverages the power of multiplexing with an application-aware decision parameter for distillation. Additionally, we presented a thorough evaluation of performance differences between one-way and multiplexed two-way protocols using relevant metrics such as the secret-key rate, number of repeaters, qubits, and gate and measurement operations. Our evaluation primarily focused on parameter regimes where one-way schemes have previously been considered advantageous. We demonstrate that the multiplexed two-way repeater scheme, in an unconstrained memory regime, outperform one-way schemes even in parameter regimes where one-way schemes have had previously been shown to be advantageous. Furthermore, these performance gains can be realized with a lower resource requirements, making two-way schemes a more attractive alternative.

While our findings suggest that multiplexed two-way schemes are potentially a near universal choice across various parameter regimes, the performance achieved in our analysis may be sub-optimal. Our study focused on basic protocols and requires further exploration to identify additional areas for improvement. For instance, our current analysis does not utilize any adaptive mechanisms at the link level for decision-making to optimize overall performance. Additionally, we only considered a basic DEJMPS protocol with a maximum of a single

(a)



(b)

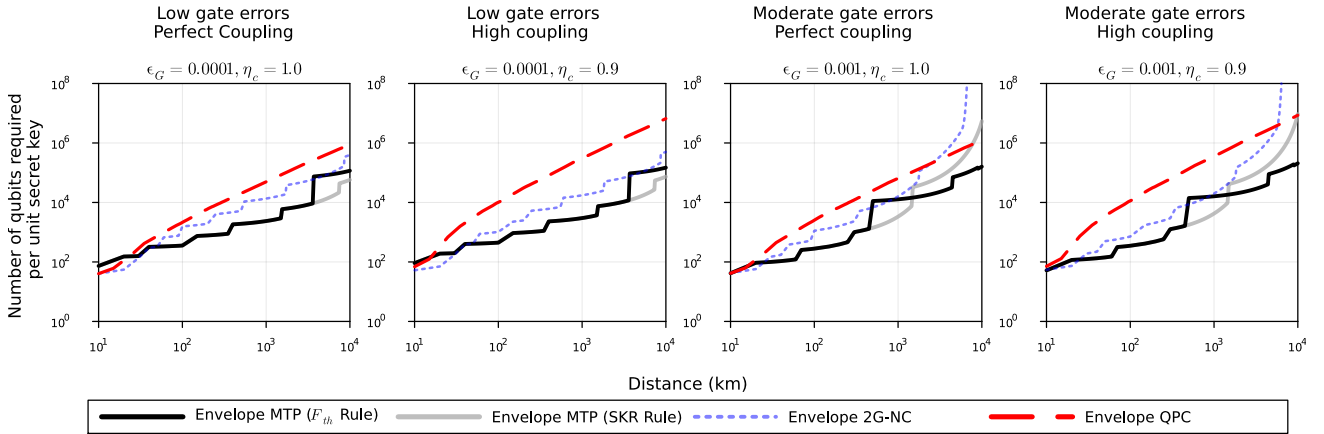


Figure 6: Number of (a) repeaters, and (b) qubits required per burst for each unit secret-key delivered for optimal performance for one- and two-way repeater architectures. The red dashed line shows the number of repeaters required for the optimal Quantum Parity Code (QPC), the blue dotted line shows the number of repeaters required for optimal performance for 2G-NC, the black and the gray solid lines are the envelopes for the number of repeaters required for the optimal performing multiplexed two-way schemes (MTP) using a $F_{th} = 0.95$ and a SKR based distillation decision rule respectively. To note, we do not consider the ancilla qubits required for state preparation, or teleportation-based error correction for QPC, and the estimation presented here is a lower bound. For all long distance parameter regimes considered, the MTP requires significantly less number of repeaters, and number of qubits than the QPC. Compared to the 2G-NC, the MTP (SKR rule) scheme require a similar number of repeaters but less number of qubits for delivering unit secret-key. To note, MTP using the F_{th} rule requires slightly more repeaters than the MTP based on the SKR rule, and the 2G-NC protocol, but lower number of repeaters than the QPC.

round performed at any nested level. These design choices likely leave room for further performance gains using advanced distillation schemes [46] while lowering resource requirements. Moreover, our distillation scheduling may not be optimal and could be improved to enhance performance and reduce costs.

Using the analysis framework proposed in this manuscript, future work can focus on improving network performance by introducing optimizations in distillation scheduling or selecting more efficient distillation protocols. Extending this framework to an asynchronous setup or a connection-less protocol might provide interesting insights and potential improvements. We recommend exploring these extensions in future research.

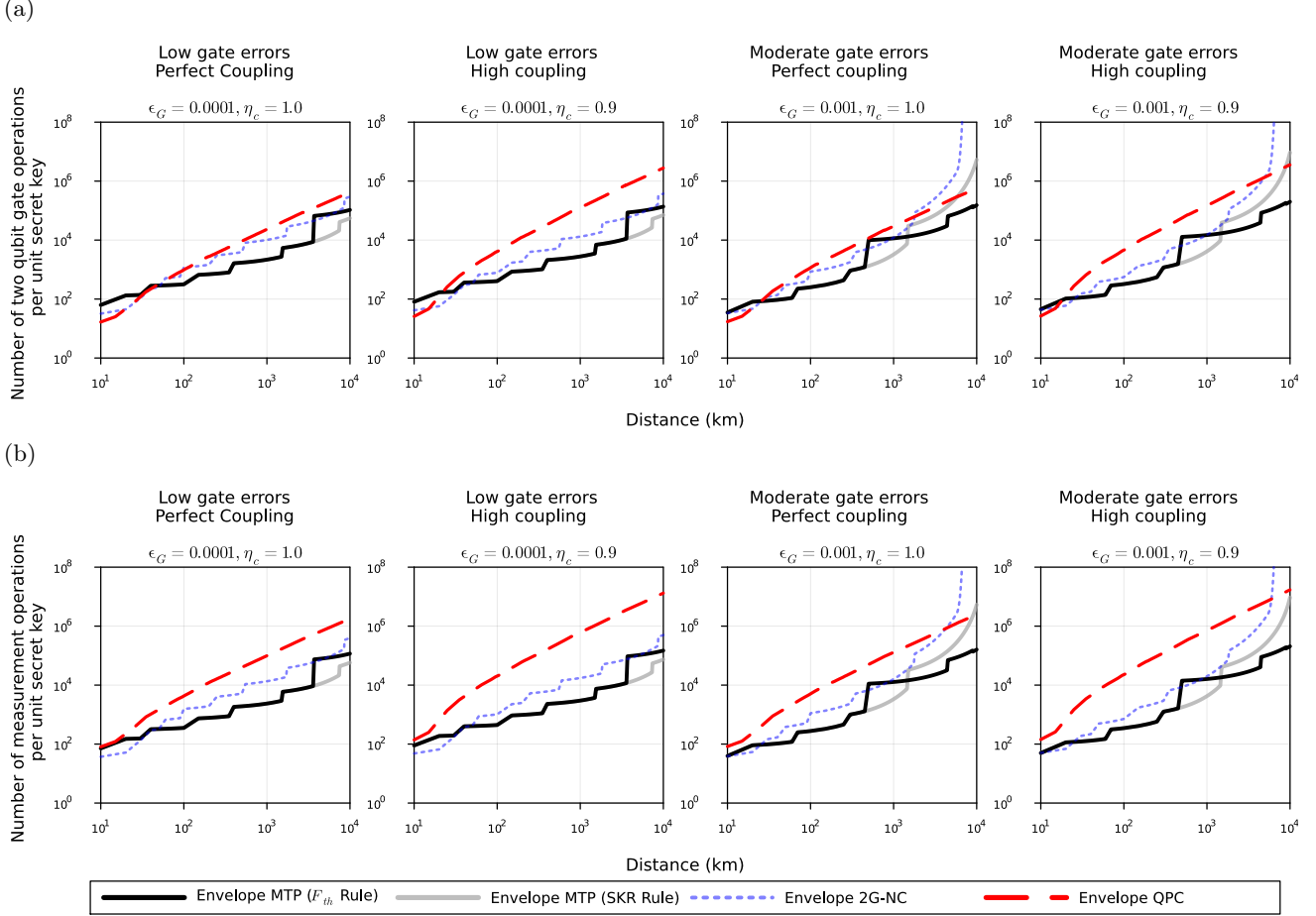


Figure 7: Number of (a) two-qubit gates, and (b) measurement operations required per burst for each unit secret-key delivered for one- and two-way repeater architectures. The red dashed line shows the number of repeaters required for the optimal Quantum Parity Code (QPC), the blue dotted line shows the number of repeaters required for optimal performance for 2G-NC, the black and the gray solid lines are the envelopes for the highest deliverable secret-key rate for multiplexed two-way schemes (MTP) using a $F_{th} = 0.95$ and a SKR based distillation decision rule respectively. To note, for QPCs, we have not considered gate operations required for state preparation or gate operations on ancilla qubits, and the estimation presented here is a lower bound. For (almost) all parameter regimes considered, the optimal QPC based protocol require higher number of two-qubit gates and measurement operations than the MTP.

6 Supplementary Materials and Data Availability

Supplementary Materials are available at this online repository[63]. All the data presented in this paper is the result of numerical simulations. The code used to generate this data is available upon reasonable request.

7 Author Contributions

DT formulated the general problem. PM designed the protocols, and conducted evaluations. PM and DT contributed to analysis. KG contributed to discussions. PM wrote the manuscript with inputs from all co-authors.

8 Competing Interests

The authors declare no competing interests.

9 Acknowledgment

We thank Saikat Guha and Alireza Shabani for their valuable comments on the project idea and intermediate results. We are especially grateful to Liang Jiang and Filip Rozpedek for their insightful feedback and suggestions on the manuscript. Additionally, we thank the Manning College of Information and Computer Sciences at the University of Massachusetts Amherst for providing access to their High Performance Computation Cluster. The authors acknowledge funding support from the NSF- ERC Center for Quantum Networks grant EEC-1941583, and DOE Grant AK0000000018297.

References

1. Degen, C. L., Reinhard, F. & Cappellaro, P. Quantum sensing. en. *Reviews of Modern Physics* **89**, 035002. ISSN: 0034-6861, 1539-0756. <http://link.aps.org/doi/10.1103/RevModPhys.89.035002> (2024) (July 2017).
2. Eldredge, Z., Foss-Feig, M., Gross, J. A., Rolston, S. L. & Gorshkov, A. V. Optimal and secure measurement protocols for quantum sensor networks. en. *Physical Review A* **97**, 042337. ISSN: 2469-9926, 2469-9934. <https://link.aps.org/doi/10.1103/PhysRevA.97.042337> (2024) (Apr. 2018).
3. Ge, W., Jacobs, K., Eldredge, Z., Gorshkov, A. V. & Foss-Feig, M. Distributed Quantum Metrology with Linear Networks and Separable Inputs. en. *Physical Review Letters* **121**, 043604. ISSN: 0031-9007, 1079-7114. <https://link.aps.org/doi/10.1103/PhysRevLett.121.043604> (2024) (July 2018).
4. Guo, X. *et al.* Distributed quantum sensing in a continuous-variable entangled network. en. *Nature Physics* **16**. Publisher: Nature Publishing Group, 281–284. ISSN: 1745-2481. <https://www.nature.com/articles/s41567-019-0743-x> (2024) (Mar. 2020).
5. Caleffi, M. *et al.* *Distributed Quantum Computing: a Survey* en. arXiv:2212.10609 [quant-ph]. Dec. 2022. <http://arxiv.org/abs/2212.10609> (2024).
6. De Andrade, M. G., Panigrahy, N. K., Dai, W., Guha, S. & Towsley, D. *Universal Quantum Walk Control Plane for Quantum Networks* en. arXiv:2307.06492 [quant-ph]. July 2023. <http://arxiv.org/abs/2307.06492> (2024).
7. Pirandola, S. *et al.* Advances in Quantum Cryptography. en. *Advances in Optics and Photonics* **12**. arXiv:1906.01645 [math-ph, physics:physics, physics:quant-ph], 1012. ISSN: 1943-8206. <http://arxiv.org/abs/1906.01645> (2024) (Dec. 2020).
8. Pan, D. *et al.* *The Evolution of Quantum Secure Direct Communication: On the Road to the Qinternet* en. arXiv:2311.13974 [quant-ph]. Nov. 2023. <http://arxiv.org/abs/2311.13974> (2024).
9. Hillery, M., Bužek, V. & Berthiaume, A. Quantum secret sharing. *Physical Review A* **59**. Publisher: American Physical Society, 1829–1834. <https://link.aps.org/doi/10.1103/PhysRevA.59.1829> (2024) (Mar. 1999).
10. Markham, D. & Sanders, B. C. Graph states for quantum secret sharing. *Physical Review A* **78**. Publisher: American Physical Society, 042309. <https://link.aps.org/doi/10.1103/PhysRevA.78.042309> (2024) (Oct. 2008).
11. Pirandola, S., Laurenza, R., Ottaviani, C. & Banchi, L. Fundamental limits of repeaterless quantum communications. en. *Nature Communications* **8**. Publisher: Nature Publishing Group, 15043. ISSN: 2041-1723. <https://www.nature.com/articles/ncomms15043> (2024) (Apr. 2017).

12. Takeoka, M., Guha, S. & Wilde, M. M. Fundamental rate-loss tradeoff for optical quantum key distribution. en. *Nature Communications* **5**. arXiv:1504.06390 [quant-ph], 5235. ISSN: 2041-1723. <http://arxiv.org/abs/1504.06390> (2024) (Oct. 2014).
13. Munro, W. J., Azuma, K., Tamaki, K. & Nemoto, K. Inside Quantum Repeaters. *IEEE Journal of Selected Topics in Quantum Electronics* **21**. Conference Name: IEEE Journal of Selected Topics in Quantum Electronics, 78–90. ISSN: 1558-4542. <https://ieeexplore.ieee.org/document/7010905> (2024) (May 2015).
14. Muralidharan, S. *et al.* Optimal architectures for long distance quantum communication. en. *Scientific Reports* **6**, 20463. ISSN: 2045-2322. <http://www.nature.com/articles/srep20463> (2022) (Apr. 2016).
15. Muralidharan, S., Kim, J., Lütkenhaus, N., Lukin, M. D. & Jiang, L. Ultrafast and Fault-Tolerant Quantum Communication across Long Distances. *Physical Review Letters* **112**. Publisher: American Physical Society, 250501. <https://link.aps.org/doi/10.1103/PhysRevLett.112.250501> (2023) (June 2014).
16. Niu, D., Zhang, Y., Shabani, A. & Shapourian, H. All-photonic one-way quantum repeaters with measurement-based error correction. en. *npj Quantum Information* **9**. Number: 1 Publisher: Nature Publishing Group, 1–9. ISSN: 2056-6387. <https://www.nature.com/articles/s41534-023-00775-9> (2024) (Oct. 2023).
17. *The Next Decade in Quantum Computing—and How to Play* en. Aug. 2020. <https://www.bcg.com/publications/2018/next-decade-quantum-computing-how-play> (2024).
18. Wang, P. *et al.* Single ion qubit with estimated coherence time exceeding one hour. en. *Nature Communications* **12**. Number: 1 Publisher: Nature Publishing Group, 233. ISSN: 2041-1723. <https://www.nature.com/articles/s41467-020-20330-w> (2024) (Jan. 2021).
19. Dudin, Y. O., Li, L. & Kuzmich, A. Light storage on the time scale of a minute. *Physical Review A* **87**. Publisher: American Physical Society, 031801. <https://link.aps.org/doi/10.1103/PhysRevA.87.031801> (2024) (Mar. 2013).
20. Razavi, M., Piani, M. & Lütkenhaus, N. Quantum repeaters with imperfect memories: Cost and scalability. en. *Physical Review A* **80**, 032301. ISSN: 1050-2947, 1094-1622. <https://link.aps.org/doi/10.1103/PhysRevA.80.032301> (2024) (Sept. 2009).
21. Guha, S. *et al.* Rate-loss analysis of an efficient quantum repeater architecture. en. *Physical Review A* **92**. arXiv:1404.7183 [quant-ph], 022357. ISSN: 1050-2947, 1094-1622. <http://arxiv.org/abs/1404.7183> (2023) (Aug. 2015).
22. Dhara, P., Patil, A., Krovi, H. & Guha, S. Subexponential rate versus distance with time-multiplexed quantum repeaters. en. *Physical Review A* **104**, 052612. ISSN: 2469-9926, 2469-9934. <https://link.aps.org/doi/10.1103/PhysRevA.104.052612> (2024) (Nov. 2021).
23. Dhara, P., Linke, N. M., Waks, E., Guha, S. & Seshadreesan, K. P. Multiplexed quantum repeaters based on dual-species trapped-ion systems. en. *Physical Review A* **105**, 022623. ISSN: 2469-9926, 2469-9934. <https://link.aps.org/doi/10.1103/PhysRevA.105.022623> (2024) (Feb. 2022).
24. Collins, O. A., Jenkins, S. D., Kuzmich, A. & Kennedy, T. A. B. Multiplexed Memory-Insensitive Quantum Repeaters. en. *Physical Review Letters* **98**, 060502. ISSN: 0031-9007, 1079-7114. <https://link.aps.org/doi/10.1103/PhysRevLett.98.060502> (2024) (Feb. 2007).
25. Razavi, M., Thompson, K., Farmanbar, H., Piani, M. & Lütkenhaus, N. *Physical and architectural considerations in quantum repeaters* in *Quantum Communications Realized II* **7236** (SPIE, Jan. 2009), 18–30. <https://www.spiedigitallibrary.org/conference-proceedings-of-spie/7236/723603/Physical-and-architectural-considerations-in-quantum-repeaters/10.1117/12.811880.full> (2024).
26. Rozpędek, F., Seshadreesan, K. P., Polakos, P., Jiang, L. & Guha, S. All-photonic Gottesman-Kitaev-Preskill-qubit repeater using analog-information-assisted multiplexed entanglement ranking. en. *Physical Review Research* **5**, 043056. ISSN: 2643-1564. <https://link.aps.org/doi/10.1103/PhysRevResearch.5.043056> (2024) (Oct. 2023).

27. Li, B., Goodenough, K., Rozpędek, F. & Jiang, L. *Generalized quantum repeater graph states* en. arXiv:2407.01429 [quant-ph]. July 2024. <http://arxiv.org/abs/2407.01429> (2024).
28. Munro, W. J., Harrison, K. A., Stephens, A. M., Devitt, S. J. & Nemoto, K. From quantum multiplexing to high-performance quantum networking. en. *Nature Photonics* **4**, 792–796. ISSN: 1749-4885, 1749-4893. <http://www.nature.com/articles/nphoton.2010.213> (2022) (Nov. 2010).
29. Piparo, N. L., Hanks, M., Gravel, C., Nemoto, K. & Munro, W. J. Resource reduction for distributed quantum information processing using quantum multiplexed photons. en. *Physical Review Letters* **124**, arXiv:1907.02240 [quant-ph], 210503. ISSN: 0031-9007, 1079-7114. <http://arxiv.org/abs/1907.02240> (2024) (May 2020).
30. Chen, K. C. *et al.* Zero-Added-Loss Entangled-Photon Multiplexing for Ground- and Space-Based Quantum Networks. en. *Physical Review Applied* **19**, 054029. ISSN: 2331-7019. <https://link.aps.org/doi/10.1103/PhysRevApplied.19.054029> (2024) (May 2023).
31. Piparo, N. L., Munro, W. J. & Nemoto, K. Quantum multiplexing. en. *Physical Review A* **99**, arXiv:1807.02940 [quant-ph], 022337. ISSN: 2469-9926, 2469-9934. <http://arxiv.org/abs/1807.02940> (2024) (Feb. 2019).
32. Nishio, S., Lo Piparo, N., Hanks, M., Munro, W. J. & Nemoto, K. Resource reduction in multiplexed high-dimensional quantum Reed-Solomon codes. en. *Physical Review A* **107**, 032620. ISSN: 2469-9926, 2469-9934. <https://link.aps.org/doi/10.1103/PhysRevA.107.032620> (2024) (Mar. 2023).
33. Nishio, S. *et al.* *Multiplexed Quantum Communication with Surface and Hypergraph Product Codes* en. arXiv:2406.08832 [quant-ph]. June 2024. <http://arxiv.org/abs/2406.08832> (2024).
34. Miki, S., Yamashita, T., Wang, Z. & Terai, H. A 64-pixel NbTiN superconducting nanowire single-photon detector array for spatially resolved photon detection. en. *Optics Express* **22**, 7811. ISSN: 1094-4087. <https://opg.optica.org/oe/abstract.cfm?uri=oe-22-7-7811> (2024) (Apr. 2014).
35. Dür, W., Briegel, H.-J., Cirac, J. I. & Zoller, P. Quantum repeaters based on entanglement purification. en. *Physical Review A* **59**, 169–181. ISSN: 1050-2947, 1094-1622. <https://link.aps.org/doi/10.1103/PhysRevA.59.169> (2024) (Jan. 1999).
36. Hartmann, L., Kraus, B., Briegel, H.-J. & Dür, W. Role of memory errors in quantum repeaters. en. *Physical Review A* **75**, 032310. ISSN: 1050-2947, 1094-1622. <https://link.aps.org/doi/10.1103/PhysRevA.75.032310> (2023) (Mar. 2007).
37. Kozłowski, W., Dahlberg, A. & Wehner, S. *Designing a quantum network protocol* en. in *Proceedings of the 16th International Conference on emerging Networking EXperiments and Technologies* (ACM, Barcelona Spain, Nov. 2020), 1–16. ISBN: 978-1-4503-7948-9. <https://dl.acm.org/doi/10.1145/3386367.3431293> (2024).
38. Pouryousef, S., Shapourian, H. & Towsley, D. *Analysis of Asynchronous Protocols for Entanglement Distribution in Quantum Networks* en. arXiv:2405.02406 [quant-ph]. May 2024. <http://arxiv.org/abs/2405.02406> (2024).
39. Xiao, Z. *et al.* A Connectionless Entanglement Distribution Protocol Design in Quantum Networks. en. *IEEE Network* **38**, 131–139. ISSN: 0890-8044, 1558-156X. <https://ieeexplore.ieee.org/document/10274626/> (2024) (Jan. 2024).
40. Bacciottini, L., Lenzini, L., Mingozzi, E. & Anastasi, G. REDiP: Ranked Entanglement Distribution Protocol for the Quantum Internet. en. *IEEE Open Journal of the Communications Society* **5**, 397–411. ISSN: 2644-125X. <https://ieeexplore.ieee.org/document/10366853/> (2024) (2024).
41. Duan, L.-M., Lukin, M. D., Cirac, J. I. & Zoller, P. Long-distance quantum communication with atomic ensembles and linear optics. en. *Nature* **414**. Publisher: Nature Publishing Group, 413–418. ISSN: 1476-4687. <https://www.nature.com/articles/35106500> (2024) (Nov. 2001).
42. Briegel, H.-J., Dür, W., Cirac, J. I. & Zoller, P. Quantum Repeaters: The Role of Imperfect Local Operations in Quantum Communication. *Physical Review Letters* **81**. Publisher: American Physical Society, 5932–5935. <https://link.aps.org/doi/10.1103/PhysRevLett.81.5932> (2024) (Dec. 1998).

43. Rozpedek, F. *et al.* Optimizing practical entanglement distillation. en. *Physical Review A* **97**, 062333. ISSN: 2469-9926, 2469-9934. <https://link.aps.org/doi/10.1103/PhysRevA.97.062333> (2024) (June 2018).
44. Krastanov, S., Albert, V. V. & Jiang, L. Optimized Entanglement Purification. en-GB. *Quantum* **3**. Publisher: Verein zur Förderung des Open Access Publizierens in den Quantenwissenschaften, 123. <https://quantum-journal.org/papers/q-2019-02-18-123/> (2024) (Feb. 2019).
45. Jansen, S., Goodenough, K., de Bone, S., Gijswijt, D. & Elkouss, D. Enumerating all bilocal Clifford distillation protocols through symmetry reduction. en. *Quantum* **6**. arXiv:2103.03669 [quant-ph], 715. ISSN: 2521-327X. <http://arxiv.org/abs/2103.03669> (2024) (May 2022).
46. Goodenough, K. *et al.* Near-term n to k distillation protocols using graph codes. en. *IEEE Journal on Selected Areas in Communications*, 1–1. ISSN: 0733-8716, 1558-0008. <https://ieeexplore.ieee.org/document/10479665/> (2024) (2024).
47. Deutsch, D. *et al.* Quantum Privacy Amplification and the Security of Quantum Cryptography over Noisy Channels. en. *Physical Review Letters* **77**, 2818–2821. ISSN: 0031-9007, 1079-7114. <https://link.aps.org/doi/10.1103/PhysRevLett.77.2818> (2024) (Sept. 1996).
48. Munro, W. J., Stephens, A. M., Devitt, S. J., Harrison, K. A. & Nemoto, K. *Quantum communication without the necessity of quantum memories* en. arXiv:1306.4137 [quant-ph]. June 2013. <http://arxiv.org/abs/1306.4137> (2024).
49. Jiang, L. *et al.* Quantum repeater with encoding. *Physical Review A* **79**. Publisher: American Physical Society, 032325. <https://link.aps.org/doi/10.1103/PhysRevA.79.032325> (2024) (Mar. 2009).
50. Ralph, T. C., Hayes, A. J. F. & Gilchrist, A. Loss Tolerant Optical Qubits. en. *Physical Review Letters* **95**. arXiv:quant-ph/0501184, 100501. ISSN: 0031-9007, 1079-7114. <http://arxiv.org/abs/quant-ph/0501184> (2024) (Aug. 2005).
51. Namiki, R., Jiang, L., Kim, J. & Lütkenhaus, N. Role of syndrome information on a one-way quantum repeater using teleportation-based error correction. en. *Physical Review A* **94**, 052304. ISSN: 2469-9926, 2469-9934. <https://link.aps.org/doi/10.1103/PhysRevA.94.052304> (2023) (Nov. 2016).
52. Bennett, C. H. & Brassard, G. Quantum cryptography: Public key distribution and coin tossing. *Theoretical Computer Science. Theoretical Aspects of Quantum Cryptography – celebrating 30 years of BB84* **560**, 7–11. ISSN: 0304-3975. <https://www.sciencedirect.com/science/article/pii/S0304397514004241> (2024) (Dec. 2014).
53. Pino, J. M. *et al.* Demonstration of the trapped-ion quantum CCD computer architecture. en. *Nature* **592**. Number: 7853 Publisher: Nature Publishing Group, 209–213. ISSN: 1476-4687. <https://www.nature.com/articles/s41586-021-03318-4> (2024) (Apr. 2021).
54. Bluvstein, D. *et al.* *Logical quantum processor based on reconfigurable atom arrays* en. arXiv:2312.03982 [cond-mat, physics:physics, physics:quant-ph]. Dec. 2023. <http://arxiv.org/abs/2312.03982> (2024).
55. Reiserer, A. & Rempe, G. Cavity-based quantum networks with single atoms and optical photons. en. *Reviews of Modern Physics* **87**, 1379–1418. ISSN: 0034-6861, 1539-0756. <https://link.aps.org/doi/10.1103/RevModPhys.87.1379> (2024) (Dec. 2015).
56. Brekenfeld, M., Niemietz, D., Christesen, J. D. & Rempe, G. A Quantum Network Node with Crossed Optical Fibre Cavities. en. *Nature Physics* **16**. arXiv:2004.08832 [quant-ph], 647–651. ISSN: 1745-2473, 1745-2481. <http://arxiv.org/abs/2004.08832> (2024) (June 2020).
57. Borne, A., Northup, T. E., Blatt, R. & Dayan, B. Efficient ion-photon qubit SWAP gate in realistic ion cavity-QED systems without strong coupling. EN. *Optics Express* **28**. Publisher: Optica Publishing Group, 11822–11839. ISSN: 1094-4087. <https://opg.optica.org/oe/abstract.cfm?uri=oe-28-8-11822> (2024) (Apr. 2020).

58. Asaoka, R., Utsugi, T., Tokunaga, Y., Kanamoto, R. & Aoki, T. *Optimization of a cavity-QED system for fast two-qubit gates* en. in *2021 Conference on Lasers and Electro-Optics Europe & European Quantum Electronics Conference (CLEO/Europe-EQEC)* (IEEE, Munich, Germany, June 2021), 1–1. ISBN: 978-1-66541-876-8. <https://ieeexplore.ieee.org/document/9542055/> (2024).
59. Solak, L. O. R., Rossatto, D. Z. & Villas-Boas, C. J. *Universal Quantum Computation Using Atoms in Cross-Cavity Systems* en. arXiv:2308.14881 [quant-ph]. Aug. 2023. <http://arxiv.org/abs/2308.14881> (2024).
60. Kollath-Bönig, J. S. *et al.* *Fast storage of photons in cavity-assisted quantum memories* en. arXiv:2401.17394 [quant-ph]. Feb. 2024. <http://arxiv.org/abs/2401.17394> (2024).
61. Borregaard, J., Kómár, P., Kessler, E. M., Lukin, M. D. & Sørensen, A. S. Long-distance entanglement distribution using individual atoms in optical cavities. en. *Physical Review A* **92**, 012307. ISSN: 1050-2947, 1094-1622. <https://link.aps.org/doi/10.1103/PhysRevA.92.012307> (2024) (July 2015).
62. Van Meter, R., Satoh, T., Ladd, T. D., Munro, W. J. & Nemoto, K. Path Selection for Quantum Repeater Networks. en. *Networking Science* **3**. arXiv:1206.5655 [quant-ph], 82–95. ISSN: 2076-0310, 2076-0329. <http://arxiv.org/abs/1206.5655> (2024) (Dec. 2013).
63. <https://github.com/mantri-prateek/multiplexed-twoway-protocol.git>.

Appendix A Process models

This appendix outlines the models assumed for various processes and operations associated with the proposed Multiplexed Two-way Scheme. As mentioned in Section 2, we consider a linear network with each repeater station equipped with a large number of optically active memories or emitters.

A.I Elementary link generation

Emitters located at neighboring repeaters emit photons entangled with their state. These photons are then sent to a station located mid-way between the repeaters supporting an array of Bell State Analyzers (Section 2.1.3). These Bell state analysers perform probabilistic Bell state measurements, with the probability of successful generation of an elementary link given by

$$\pi_0 = \frac{1}{2}\eta_c^2 e^{-L_0/L_{att}}, \quad (\text{A.1})$$

where η_c is the coupling efficiency, L_0 is the inter-repeater distance, and L_{att} is the attenuation length taken as 20 km in this manuscript.

A.II Fidelity

We model the generated quantum elementary link (represented as the two-qubit quantum state ρ) as a Bell-diagonal state. This state can be represented as a linear combination of the four Bell states -

$$\rho = a |\phi^+\rangle \langle \phi^+| + b |\phi^-\rangle \langle \phi^-| + c |\psi^+\rangle \langle \psi^+| + d |\psi^-\rangle \langle \psi^-|, \quad (\text{A.2})$$

where $|\varphi^\pm\rangle = \frac{1}{\sqrt{2}}(|00\rangle \pm |11\rangle)$ and $|\psi^\pm\rangle = \frac{1}{\sqrt{2}}(|01\rangle \pm |10\rangle)$ are the four Bell states. As a shorthand, we represent this state as the state tuple $\{a, b, c, d\}$ corresponding to the probabilities of each of the four Bell states. Fidelity of ρ is given by $F \equiv \langle \phi^+ | \rho | \phi^+ \rangle = a$.

A.III Gate operations

Local two-qubit gates, such as the CNOT gate, are characterized by the gate error parameter ϵ_G . This parameter indicates the probability that the gate operation will result into a maximally mixed state. Conversely, with probability $1 - \epsilon_G$, the gate performs the intended operation correctly. This can be mathematically expressed as -

$$\mathcal{N}_{\bar{U}_{ij}}(\rho) = (1 - \epsilon_G)U_{ij}\rho U_{ij}^\dagger + \frac{\epsilon_G}{4}\text{Tr}_{ij}[\rho] \otimes I_{ij}, \quad (\text{A.3})$$

where U_{ij} represents the ideal two-qubit operation on qubits i and j , $\text{Tr}_{ij}[\rho]$ denotes the partial trace over qubits i and j , and I_{ij} is the identity operator.

A.IV Measurement operations

Measurement errors in qubits are described by the measurement error ξ , which quantifies the probability of an incorrect measurement outcome. The error models for projective measurements on the states $|0\rangle$ and $|1\rangle$ are given by-

$$P_0 = (1 - \xi)|0\rangle\langle 0| + \xi|1\rangle\langle 1|, \quad (\text{A.4})$$

$$P_1 = (1 - \xi)|1\rangle\langle 1| + \xi|0\rangle\langle 0|. \quad (\text{A.5})$$

To mitigate measurement errors, an ancillary qubit can be introduced and both the data qubit and the ancillary qubit can be measured. If the measurement outcomes differ, it is interpreted as a loss error on the qubit. Using the same argument forwarded in Muralidharan *et. al* [14], we assume the effective measurement error to be given by $0.25\epsilon_G$, in case of a match of measurement outcomes. This is reasonable since the gate error rates considered range between 10^{-4} and 10^{-2} , making the contribution of measurement errors to the overall error rate to be minimal.

A.V Memory Decoherence

Quantum memories undergo decoherence with time. While this decoherence is commonly modelled to be either due to relaxing (T_1) or dephasing (T_2), we only include the effects of dephasing in our analysis. Because of decoherence, the state tuple $\{a, b, c, d\}$ is updated in the following manner to $\{a_{dec}, b_{dec}, c_{dec}, d_{dec}\}$, where

$$\begin{aligned} a_{dec} &= \lambda_{dec}a + (1 - \lambda_{dec})b, \\ b_{dec} &= \lambda_{dec}b + (1 - \lambda_{dec})a, \\ c_{dec} &= \lambda_{dec}c + (1 - \lambda_{dec})d, \\ d_{dec} &= \lambda_{dec}d + (1 - \lambda_{dec})c. \end{aligned} \quad (\text{A.6})$$

Here $\lambda_{dec} = \frac{1+e^{-2t/T_2}}{2}$ [13], and t is the time that the state ρ is stored in memory.

A.VI Distillation

For two links with state tuple - $\{a_1, b_1, c_1, d_1\}$ and $\{a_2, b_2, c_2, d_2\}$, the DEJMPS [14, 47] distillation protocol leads to the tuple $\{a, b, c, d\}$ with a probability of success given by p^\uparrow

$$p^\dagger = (1 - \epsilon_G)^2 \{ [\xi^2 + (1 - \xi)^2] [(a_1 + d_1)(a_2 + d_2) + (b_1 + c_1)(c_2 + b_2)] + 2\xi(1 - \xi) [(a_1 + d_1)(b_2 + c_2) + (b_1 + c_1)(a_2 + d_2)] \} + \frac{1}{2} [1 - (1 - \epsilon_G)^2] \quad (\text{A.7})$$

$$\begin{aligned} a &= \frac{1}{p^\dagger} \{ (1 - \epsilon_G)^2 [(\xi^2 + (1 - \xi)^2)(a_1 a_2 + d_1 d_2) + 2\xi(1 - \xi)(a_1 c_2 + d_1 b_2)] \} + \frac{1}{8} [1 - (1 - \epsilon_G)^2] \\ b &= \frac{1}{p^\dagger} \{ (1 - \epsilon_G)^2 [(\xi^2 + (1 - \xi)^2)(a_1 d_2 + d_1 a_2) + 2\xi(1 - \xi)(a_1 b_2 + d_1 c_2)] \} + \frac{1}{8} [1 - (1 - \epsilon_G)^2] \\ c &= \frac{1}{p^\dagger} \{ (1 - \epsilon_G)^2 [(\xi^2 + (1 - \xi)^2)(b_1 b_2 + c_1 c_2) + 2\xi(1 - \xi)(b_1 d_2 + c_1 a_2)] \} + \frac{1}{8} [1 - (1 - \epsilon_G)^2] \\ d &= \frac{1}{p^\dagger} \{ (1 - \epsilon_G)^2 [(\xi^2 + (1 - \xi)^2)(b_1 c_2 + c_1 b_2) + 2\xi(1 - \xi)(b_1 a_2 + c_1 d_2)] \} + \frac{1}{8} [1 - (1 - \epsilon_G)^2]. \end{aligned} \quad (\text{A.8})$$

A.VII Entanglement Swapping

Entanglement swapping is used in two-way quantum networks to extend the distance of entanglement. With imperfect CNOT operation and measurements, the state $\{a, b, c, d\}$ obtained from deterministically swapping the input pairs $\{a_1, b_1, c_1, d_1\}$ and $\{a_2, b_2, c_2, d_2\}$ is

$$\begin{aligned} a &= (1 - \epsilon_G) \{ (1 - \xi)^2 (a_1 a_2 + b_1 b_2 + c_1 c_2 + d_1 d_2) + \xi(1 - \xi) [(a_1 + d_1)(b_2 + c_2) + (b_1 + c_1)(a_2 + d_2)] + \xi^2 (a_1 d_2 + d_1 a_2 + b_1 c_2 + c_1 b_2) \} + \frac{\epsilon_G}{4} \\ b &= (1 - \epsilon_G) \{ (1 - \xi)^2 (a_1 b_2 + b_1 a_2 + c_1 d_2 + d_1 c_2) + \xi(1 - \xi) [(a_1 + d_1)(a_2 + d_2) + (b_1 + c_1)(b_2 + c_2)] + \xi^2 (a_1 c_2 + c_1 a_2 + b_1 d_2 + d_1 b_2) \} + \frac{\epsilon_G}{4} \\ c &= (1 - \epsilon_G) \{ (1 - \xi)^2 (a_1 c_2 + c_1 a_2 + b_1 d_2 + d_1 b_2) + \xi(1 - \xi) [(a_1 + d_1)(a_2 + d_2) + (b_1 + c_1)(b_2 + c_2)] + \xi^2 (a_1 b_2 + b_1 a_2 + c_1 d_2 + d_1 c_2) \} + \frac{\epsilon_G}{4} \\ d &= (1 - \epsilon_G) \{ (1 - \xi)^2 (a_1 d_2 + d_1 a_2 + c_1 b_2 + b_1 c_2) + \xi(1 - \xi) [(a_1 + d_1)(b_2 + c_2) + (b_1 + c_1)(a_2 + d_2)] + \xi^2 (a_1 a_2 + b_1 b_2 + c_1 c_2 + d_1 d_2) \} + \frac{\epsilon_G}{4}. \end{aligned} \quad (\text{A.9})$$

A.VIII Secret-key rate

The secure key generation rate, R_{secret} (sbit/s), can be written as

$$R_{secret} = P_{succ} \cdot r_{secure} \cdot \frac{1}{t_{max}}, \quad (\text{A.10})$$

where P_{succ} is the overall success probability of the protocol, t_{max} is the maximum time taken to generate a Bell pair between the two parties, and r_{secure} is the asymptotic secure fraction in the fully asymmetric version using the one-way BB84 protocol [52],

$$r_{secure}(\rho) = \max[1 - h(Q_X) - h(Q_Z), 0], \quad (\text{A.11})$$

where $\{Q_{X/Z}\}$ is the quantum bit error rate (QBER) for phase and bit flips, and can be calculated from the density matrix of the entangled state ρ shared by Alice and Bob in the end. Here,

$$h(Q_{\{X/Z\}}) = -Q_{\{X/Z\}} \log_2 Q_{\{X/Z\}} - (1 - Q_{\{X/Z\}}) \log_2 (1 - Q_{\{X/Z\}})$$

is the binary entropy function. In Muralidharan et al. [14], an average for quantum bit error rate is taken with $Q = \frac{Q_X + Q_Z}{2}$, and secure rate is approximated as $r_{secure} = \max[1 - 2h(Q), 0]$. For our analysis, we assume

pipelining, and allow for an arbitrary number of bursts in unit time-frame. For this we define the quantity Secret-key rate per burst as

$$SKR = \mathbb{E}(Y) \cdot r_{secure}, \quad (\text{A.12})$$

where Y is the number of Bell pairs shared between two parties. Since QPC and MTP use different number of elementary channels, we further modify this quantity to define the metric of Secret-key rate per channel use per burst-

$$SKR \text{ (per channel use)} = \frac{\mathbb{E}(Y) \cdot r_{secure}}{M}, \quad (\text{A.13})$$

where M denote the number of multiplexed channels available at each elementary link, and in the case of (n, m) QPC, M is the total number of physical qubits encoding one logical qubit i.e. $M = nm$.

Appendix B Recursive formulation of the probability distribution

We consider a linear network with $N = 2^n$ links. Let $M = m2^{n+1}$ denote the number of multiplexed channels¹⁰ available at each elementary link in a single shot, with $m \geq 1$. We consider a nested pumping distillation protocol that performs at most one distillation round at each level.

Let Y_i denote the number of Bell pairs on a segment at level i with $p_{i,k} = P(Y_i = k)$ denoting the probability of having exactly k Bell pairs at level i . Let π_0 denote the probability that a link-level Bell pair generation attempt succeeds, and let $\bar{\pi}_0 = 1 - \pi_0$. Then,

$$p_{0,k} = \binom{M}{k} \pi_0^k \bar{\pi}_0^{M-k}, \quad k = 0, 1, \dots, M. \quad (\text{B.14})$$

B.I Multiplexing with exactly one success - 2GNC

For 2G-NC, the focus is on creating at least one bell pair in all segments. Further, using a similar setup assumed in [14], it is assumed that there are no distillation operations, and since swapping operations are deterministic we perform a network wide swap simulatenously on the single link created, thus creating an end-to-end bell pair with a success probability,

$$\begin{aligned} \text{Success Prob.}_{(2GNC)} &= \left(\sum_{k=1}^M p_{0,k} \right)^N, \quad k = 0, 1, \dots, M \\ &= \left(\sum_{k=1}^M p_{0,k} \binom{M}{k} \pi_0^k \bar{\pi}_0^{M-k} \right)^N, \text{ using equation (B.14)} \\ &= \left(1 - p_{0,0} \right)^N \\ &= \left(1 - \bar{\pi}_0^M \right)^N \end{aligned} \quad (\text{B.15})$$

B.II Multiplexing with more than one success

B.II.1 Using DEJMPS distillation protocol

In order to calculate $p_{i,k}$, we first determine the effect of a distillation operation at level i whenever it is performed. This is captured by $q_{i,k}$,

$$q_{i,k} = P(X_i = k) = \sum_{j=2k}^{M/2^i} p_{i,j} \binom{\lfloor j/2 \rfloor}{k} d_i^k \bar{d}_i^{\lfloor j/2 \rfloor - k}, \quad i \in \{0, \dots, n\}; k = 0, 1, \dots, \lfloor M/2^{i+1} \rfloor. \quad (\text{B.16})$$

¹⁰This can be relaxed if distillation is not required on all levels to M taken to be lesser than $m2^{n+1}$.

where X_i denote the number of Bell pairs produced by one distillation step at level i when performed, and d_i the probability of a successful distillation step. This equation can be extended to reflect the case when no distillation is performed at that level. That is,

$$q_{i,k} = P(X_i = k) = \begin{cases} \sum_{j=2k}^{M_i} p_{i,j} \binom{\lfloor j/2 \rfloor}{k} d_i^k \bar{d}_i^{\lfloor j/2 \rfloor - k}, & \mathcal{D}_i = 1 \\ p_{i,k}, & \mathcal{D}_i = 0 \end{cases}, \quad i = 0, \dots, n; k = 0, 1, \dots, \lfloor M_i/2 \rfloor \quad (\text{B.17})$$

where $M_i = \lfloor M/2^{\sum_{j=0}^{i-1} \mathcal{D}_j} \rfloor$ for $i > 0$, and \mathcal{D}_i is the indicator function for distillation,

$$\mathcal{D}_i = \begin{cases} 0, & \text{if no distillation at level } i \\ 1, & \text{if distillation at level } i \end{cases}, \quad i = 0, \dots, n$$

To note, for the current analysis we have a static value of $\mathcal{D}_i = 0$, when $i = n$. Now,

$$p_{i,k} = \begin{cases} (q_{i-1,k})^2 + 2q_{i-1,k} \sum_{j=k+1}^{M_i} q_{i-1,j}, & \mathcal{D}_i = 1 \\ (p_{i-1,k})^2 + 2p_{i-1,k} \sum_{j=k+1}^{M_i} p_{i-1,j}, & \mathcal{D}_i = 0 \end{cases}, \quad i = 1, \dots, n; k = 0, 1, \dots, M_i. \quad (\text{B.18})$$

We now consider a protocol that terminates whenever $Y_i < R_i$ where R_i denote a termination threshold for each level i segment. Let,

$$\begin{aligned} r_i &= \text{Probability of reset at level } i \text{ conditioned on reaching level } i, \\ p'_{i,k} &= P(Y_i = k \mid \text{no reset at levels } 0, 1, \dots, i), \\ q'_{i,k} &= \text{Probability of having } k \text{ distilled pairs conditioned on reaching level } i. \end{aligned}$$

Now,

$$r_0 = \sum_{j=0}^{R_0-1} \binom{M}{j} \pi_0^j \bar{\pi}_0^{M-j} \quad (\text{B.19})$$

and

$$p'_{0,k} = \begin{cases} \left(\binom{M}{k} \pi_0^k \bar{\pi}_0^{M-k} \right) / (1 - r_0), & k \geq R_0 \\ 0, & k < R_0 \end{cases}, \quad \forall k \in \{0, 1, \dots, M\}. \quad (\text{B.20})$$

Now, as defined earlier,

$$\begin{aligned} q'_{i,k} &= P(Y_i = k \mid \text{no reset at levels } 0, 1, \dots, i), \\ &= \begin{cases} \sum_{j=2k}^{M_i} p'_{i,j} \binom{\lfloor j/2 \rfloor}{k} d_i^k \bar{d}_i^{\lfloor j/2 \rfloor - k}, & \mathcal{D}_i = 1 \\ p'_{i,k}, & \mathcal{D}_i = 0 \end{cases}, \quad \forall k \in \{0, 1, \dots, \lfloor M_i/2 \rfloor\} \end{aligned} \quad (\text{B.21})$$

$$r_i = \begin{cases} \sum_{l=0}^{R_i-1} \left((q'_{i-1,l})^2 + 2q'_{i-1,l} \sum_{j=l+1}^{M_i} q'_{i-1,j} \right), & \mathcal{D}_i = 1 \\ 0, & \mathcal{D}_i = 0 \end{cases}, \quad \text{s.t. } R_i \leq R_{i-1} \quad \forall i \in \{1, \dots, n\} \quad (\text{B.22})$$

Now,

$$p'_{i,k} = \begin{cases} \left((q'_{i-1,k})^2 + 2q'_{i-1,k} \sum_{j=k+1}^{M_i} q'_{i-1,j} \right) / (1 - r_i), & \mathcal{D}_i = 1 \quad \& \quad k \geq R_i \\ (p'_{i-1,k})^2 + 2p'_{i-1,k} \sum_{j=k+1}^{M_i} p'_{i-1,j}, & \mathcal{D}_i = 0 \quad \& \quad k \geq R_i \\ 0, & k < R_i \end{cases}, \quad \forall k \in \{0, \dots, M_i\} \quad (\text{B.23})$$

Now, let f_i be the probability of reset at level i ,

$$f_i = \begin{cases} 1 - (1 - r_0)^N & , i = 0 \\ (1 - (1 - r_i)^{\frac{N}{2^i}}) \prod_{j=0}^{i-1} (1 - r_j)^{\frac{N}{2^j}} & , \text{otherwise} \end{cases} \quad (\text{B.24})$$

The decision to distill \mathcal{D}_i can be computed using any criterion best suited for the application. As examples, we have considered two conditions - (1) $F_{th} \underset{\mathcal{D}_i=0}{\overset{\mathcal{D}_i=1}{\geq}} F_i$ where F_i is the fidelity at the i^{th} level and F_{th} is a pre-decided threshold fidelity, (2) $SKR_i^\uparrow \underset{\mathcal{D}_i=0}{\overset{\mathcal{D}_i=1}{\geq}} SKR_i$, where SKR_i is the secret-key rate at level i without distillation, and SKR_i^\uparrow is the secret-key rate at level i after distillation. Using equation (A.12), this SKR based decision rule can be further elaborated as,

$$\begin{aligned} & SKR_i^\uparrow \underset{\mathcal{D}_i=0}{\overset{\mathcal{D}_i=1}{\geq}} SKR_i \\ \text{i.e.} \quad & r_{secure}(\rho_i^\uparrow) \cdot \mathbb{E}(Y_i^\uparrow) \underset{\mathcal{D}_i=0}{\overset{\mathcal{D}_i=1}{\geq}} r_{secure}(\rho_i) \cdot \mathbb{E}(Y_i), \end{aligned} \quad (\text{B.25})$$

where ρ_i is the two-qubit state shared between two parties before distillation at level i , Y_i^\uparrow denote the number of Bell pairs on a segment at level i after one round of distillation, ρ_i^\uparrow is the state after distillation at level i , $r_{secure}(\rho)$ denote the secret-key fraction for a two-qubit state ρ , and

$$\begin{aligned} \mathbb{E}(Y_i) &= \prod_{j=0}^i (1 - r_j)^{\frac{N}{2^j}} \cdot \sum_{k=R_i}^{M_i} k \cdot p'_{i,k} \\ \mathbb{E}(Y_i^\uparrow) &= \prod_{j=0}^i (1 - r_j)^{\frac{N}{2^j}} \cdot \sum_{k=R_i}^{\lfloor M_i/2 \rfloor} k \cdot q'_{i,k} \end{aligned} \quad (\text{B.26})$$

To note, for both cases listed above, we do not distill when equality holds.

B.II.2 Using a general n-to-k distillation protocol

To use the recursive formulation listed above, for a distillation protocol based on Steane Code, equation (B.21) can be updated to -

$$\begin{aligned} q'_{i,k} &= P(Y_i = k | \text{no reset at levels } 0, 1, \dots, i) \\ &= \begin{cases} \sum_{j=7k}^{M_i} p'_{i,j} \binom{\lfloor j/7 \rfloor}{k} d_i^k \bar{d}_i^{\lfloor j/7 \rfloor - k} & , \mathcal{D}_i = 1 \\ p'_{i,k} & , \mathcal{D}_i = 0 \end{cases}, \quad \forall k \in \{0, 1, \dots, \lfloor M_i/7 \rfloor\}, \end{aligned} \quad (\text{B.27})$$

where $M_i = M/7^{\sum_{i=0}^i \mathcal{D}_{i-1}}$, $M = m \cdot 7^{n+1}$, and $m \in \mathbb{Z}^+$. For a more general n' -to- k' protocol,

$$\begin{aligned} q'_{i,k} &= P(Y_i = k | \text{no reset at levels } 0, 1, \dots, i) \\ &= \begin{cases} \sum_{j=k \cdot \lceil n'/k' \rceil}^{M_i} p'_{i,j} \binom{\lfloor j/\lceil n'/k' \rceil \rfloor}{k} d_i^k \bar{d}_i^{\lfloor j/\lceil n'/k' \rceil \rfloor - k} & , \mathcal{D}_i = 1 \\ p'_{i,k} & , \mathcal{D}_i = 0 \end{cases}, \quad \forall k \in \{0, 1, \dots, \lfloor M_i/\lceil n'/k' \rceil \rfloor\} \end{aligned} \quad (\text{B.28})$$

where $M_i = M/(\lceil n'/k' \rceil)^{\sum_{i=0}^i \mathcal{D}_{i-1}}$, $M = m \cdot \lceil n'/k' \rceil^{n+1}$, and $m \in \mathbb{Z}^+$. Equations (B.20), (B.22), (B.23) and (B.24) will remain the same as the DEJMPS case.